

Kinetic energy constructed from exact gradient expansion of second order in uniform gas limit

Abhishek Bhattacharjee,^{1,*} Hemanadhan Myneni,^{2,†} Manoj K. Harbola,³ and Prasanjit Samal¹

¹*School of Physical Sciences, National Institute of Science Education and Research,
An OCC of Homi Bhabha National Institute, Jatni 752050, India*

²*Faculty of Industrial Engineering, Mechanical Engineering and Computer Science, University of Iceland, Reykjavík, Iceland*

³*Department of Physics, Indian Institute of Technology Kanpur, Kanpur 208016, India*

(Dated: December 24, 2025)

Orbital-Free Density Functional Theory (OFDFT) has re-emerged as a viable alternative to Kohn–Sham DFT, driven by recent advances in kinetic energy density functionals (KEDFs). Nonlocal (NL) KEDFs have significantly extended OFDFT's applicability, particularly for bulk solids, but their high computational cost and dependence of system-specific parameters limit their universality. In this work, we propose a semilocal KEDF at the Generalized Gradient Approximation (GGA) level that achieves accuracy comparable to state-of-the-art NL and meta-GGA functionals, while remaining entirely parameter-free. Our construction revives the Thomas–Fermi–von Weizsäcker (TFvW) framework by modulating the relative contributions of TF and vW terms through physically motivated constraints and preserving the exact second-order gradient expansion. Despite its simple form, the proposed functional (KGE2) performs remarkably well across both extended systems (metals and semiconductors) and finite systems (clusters), without any need for parameter tuning. These results mark a step toward a transferable, computationally efficient, and general-purpose KEDF suitable for large-scale OFDFT simulations.

I. INTRODUCTION

Since the pioneering work of Hohenberg and Kohn [1], later extended by Kohn and Sham [2], density functional theory (DFT) has become a cornerstone of *ab initio* electronic structure calculations. Initially applied to atoms and molecules [3], DFT now plays a central role in fields ranging from condensed matter physics and molecular dynamics to warm dense matter (WDM) [4, 5], and time-dependent phenomena [6–9]. The reason for this success lies in its compact formalism that offers a favorable balance between accuracy and computational efficiency.

Kohn–Sham (KS) DFT introduces orbitals to compute the kinetic energy exactly, improving accuracy but with a computational cost that scales as $\mathcal{O}(N^3)$ with the system size N [10]. In contrast, Orbital-Free DFT (OFDFT) returns to the original Hohenberg–Kohn framework, offering linear $\mathcal{O}(N)$ scaling by solving a single Euler [11–13]:

$$\frac{\delta T_s[\rho]}{\delta \rho} + v_{ext}(r) + \int \frac{\rho(\mathbf{r}')}{|\mathbf{r} - \mathbf{r}'|} d^3 \mathbf{r}' + \frac{\delta E_{xc}[\rho]}{\delta \rho} = \mu \quad (1)$$

Here T_s is the kinetic energy functional and E_{xc} is the exchange-correlation energy. The main challenge in OFDFT is to design kinetic energy density functionals (KEDFs) that are both accurate and transferable across diverse systems.

Significant progress has been made in developing nonlocal KEDFs (NL-KEDFs) [14–18], necessary for systems with inhomogeneous densities [19]. Most NL-KEDFs retain the von Weizsäcker (vW) term and incorporate linear response corrections to the Thomas–Fermi (TF) contribution:

$$T^{TF+NL}[\rho] = C_{TF} \int \int \rho^{5/6}(\mathbf{r}) \Omega(\mathbf{r} - \mathbf{r}') \rho^{5/6}(\mathbf{r}') d\mathbf{r} d\mathbf{r}' \quad (2)$$

Expanding about the homogeneous electron gas (HEG) density leads to:

$$\Omega(\mathbf{r} - \mathbf{r}') = \delta(\mathbf{r} - \mathbf{r}') + \omega(\mathbf{r} - \mathbf{r}') + \dots \quad (3)$$

Most NL-KEDFs derive $\omega(q)$ via the Lindhard response function. The general form of the kernel in Fourier space is:

$$\omega(q) = -\frac{\chi_{HEG}^{-1}(\eta) - \chi_{vW}^{-1}(\eta) - \chi_{TF}^{-1}(\eta)}{2\alpha\beta\rho_0^{\alpha+\beta-2}} \quad (4)$$

where $\eta = q/2k_F$ is dimensionless momentum variable and χ is the response function. Although NL-KEDFs are accurate for solids, especially metals, they often fail for semiconductors and finite systems due to the limitations of the HEG approximation [20, 21]. Furthermore, their dependence on tunable, system-specific parameters undermines transferability [22]. As Kohn noted, semilocal functionals can effectively capture nonlocal effects when only short-range interactions are relevant, a concept referred to as 'shortsightedness' [23].

Alternatively, the development of improved semilocal functionals that can mimic the accuracy of NL approaches remains an active area of research. Despite its simplicity, the TFvW functional is already capable of predicting bonding in both metals and semiconductors, whereas several NL-KEDFs, such as the Wang–Teter (WT) and Wang–Govind–Carter (WGC) forms, fail to do so [24, 25]. The general form of TFvW is:

$$T_s[\rho] = T_{TF}[\rho] + \lambda T_{vW}[\rho] \quad (5)$$

with $\lambda \in [0, 1]$. The vW term ensures correct exponential decay, satisfies the Kato cusp conditions, and captures the short-wavelength linear response behavior [11, 26–30].

* abhishek.bhattacharjee@niser.ac.in

† myneni@iitk.ac.in

The construction of semilocal KEDFs is further supported by the conjointness conjecture [31], which links the forms of exchange and kinetic enhancement factors. According to this conjecture, any exchange density functional approximation (DFA) can be transformed into a KEDF by tuning parameters [32, 33]. However, not all such functionals satisfy exact constraints [34]. A comprehensive list of GGA-type semilocal KEDFs is given in Ref. [34]. Most of these functionals fail to improve local quantities such as the electron density or the kinetic energy density, and often rely on error cancellation for accurate total energy predictions [34, 35].

A notable GGA-level attempt is APBEK [32], motivated by the success of PBE exchange, though it fails to reproduce the correct GE2 coefficient and Pauli positivity. Its refinement, VT84 [36] by Karasiev et al., addressed several of these deficiencies and marked the beginning of competitive semilocal KEDFs. Since then, a variety of functionals have emerged, some optimized for metals: Luo-Karasiev-Trickey (LKT) [37, 38] and others for semiconductors or localized systems Pauli-Gaussian (PG): [39–41]. For example, the PG1 functional is among the most accurate semilocal KEDFs but fails to recover exact GE in the low- s limit. Using $\mu = 1.481$ restores GE but deteriorates mechanical properties, especially for metals. Extensions such as PGS and PGSLr [40], incorporating mGGA terms, improve bulk properties and open the door to more versatile applications, despite the added computational cost and numerical instabilities when applied to finite systems. These challenges are especially relevant for clusters, where periodic codes can introduce Laplacian noise.

As discussed above, the NL-kernels often rely on the Fermi momentum k_F (see Eq. 4), typically approximated as a constant, $k_F = (3\pi^2\rho_0)^{1/3}$, where ρ_0 is the average electron density, to reduce computational cost. Only a few density-dependent kernels, such as HC [42], revHC, and LMGP, employ a local description, $k_F = (3\pi^2\rho(\mathbf{r}))^{1/3}$, which significantly increases the computational expense. However, density-independent NL kernels face fundamental challenges when applied to finite systems, where defining $\rho_0 = \rho/V_{box}$ becomes arbitrary and system-dependent. To the best of our knowledge, all non-local, density-independent kernels perform poorly for clusters, and none have been successfully applied to atomic or cluster calculations.

In 2018, two functionals, LWT and LMGP, proposed by Michel Pavellano et al. [43], introduced a method to perform calculations on finite systems with non-local kernels. These remain the only two NL functionals that provide reasonably good results for clusters. These functionals are modified versions of the WT and MGP functionals, where the Fermi wave vector (k_F) is treated as a local function of the density. To implement this, the kernel must be evaluated at every point in space, which would otherwise make the calculations prohibitively expensive. To address this, a spline interpolation technique, originally inspired by the revHC functional, was employed [44]. However, these functionals still carry certain limitations: (i) they contain parameters tuned to reproduce KS results, and (ii) they are unsuitable for solids and can therefore be considered system-dependent. In this context, semilocal functionals offer an attractive alternative for general-purpose

applications. Notably, such issues do not arise in semilocal KEDFs like TFvW, which do not include non-local terms.

In 2019, the PGint functional (and its variant PG20/9) was introduced [45] and applied to Ne and Rn atoms as well as to jellium clusters. These functionals were shown to outperform LKT in overall accuracy, but in SCF calculations over an extended set of noble-gas atoms, PGS yielded superior kinetic energies. This finding motivated us to include finite systems in our benchmark suite. Till date, PGS has been implemented and reported in an all-electron Engel code; its performance within periodic, pseudopotential-based frameworks remains to be assessed.

A robust KEDF must perform well across both solids and molecular systems. Motivated by universality and simplicity, we revisit semilocal KEDFs, aiming to construct a parameter-free, accurate and efficient functional. We benchmark our proposed GGA-level functional, KGE2, against state-of-the-art NL- and mGGA-KEDFs. Remarkably, KGE2 achieves comparable accuracy without fitting parameters and demonstrates good transferability to local systems, where most NL-KEDFs fail. Some NL functionals like LMGP or LWT are tailored for clusters but perform poorly for solids [43], limiting their general applicability. In this work, we present a detailed analysis of structural and local properties using KGE2.

The rest of the article is organized as follows: Section II outlines the construction of KGE2. Section III discusses benchmark results for bulk systems. Section III E presents an assessment for molecular clusters. We conclude in Section IV.

II. THEORY

A. Functional construction

Following the prescription of Perdew [46], we aim to construct an accurate yet simple GGA-level KEDF. To this end, we introduce the reduced density gradient $s = |\nabla\rho(r)|/2k_F\rho(r)$ as a key variable. The generic form of Eq. 2 can thus be written in terms of s as:

$$\begin{aligned} T_s^{GGA} &= \int \tau_{TF}(\rho)F_\theta(\rho, s)d\mathbf{r} + \lambda T_{vW} \\ &= \int \underbrace{\tau_{TF}[F_\theta + \lambda \frac{5}{3}s^2]}_{\tau_s} d\mathbf{r} \end{aligned} \quad (6)$$

Here, $\tau_{TF} = C_{TF}\rho^{5/3}$ is the Thomas Fermi kinetic energy density, $C_{TF} = \frac{3}{10}(3\pi^2)^{2/3}$. And F_θ is referred to as the Pauli enhancement factor emphasizing that the vW term does not incorporate any information related to the Pauli exclusion principle (PEP) [11, 21].

The construction of the functional must satisfy the correct asymptotic behaviour, guided by the following conditions:

- $\lim_{s \rightarrow \infty} \tau_s \rightarrow \tau_{vW}$
- $\lim_{s \rightarrow 0} \tau_s \rightarrow \tau_{TF} + \frac{1}{9}\tau_{vW}$
- $\tau_s \geq 0$ for all \mathbf{r}

Since τ_s is exact in the small- s limit, it is expected to obey all corresponding exact conditions in that region. Based on these considerations, we propose a new enhancement factor

$$F_\theta = \frac{1}{1 + \alpha s^2} \quad (7)$$

Here, $F_\theta = \frac{1}{1 + \alpha s^2}$ serves as the Pauli enhancement factor, and the parameter α is chosen as 1.481 to accurately reproduce GEA in the small- s limit. As mentioned in sec. I, the previously proposed similar semilocal enhancement factors are PG and LKT has the forms $F_\theta^{PG} = \exp(-\mu s^2)$ [39] and $F_\theta^{LKT} = \frac{1}{\cosh(\alpha s)}$ [37] respectively. All three forms are plotted in Fig. 1 for visual comparison. Expansion in the low- s limit makes it clear that only PGS and KGE2 converge to GE2 respecting the second constraint: $\lim_{s \rightarrow 0} \tau_s \rightarrow \tau_{TF} + \frac{1}{9} \tau_{vW}$. Thus the key difference between KGE2 and other semilocals lies in the recovering of exact GE2 in low- s regions.

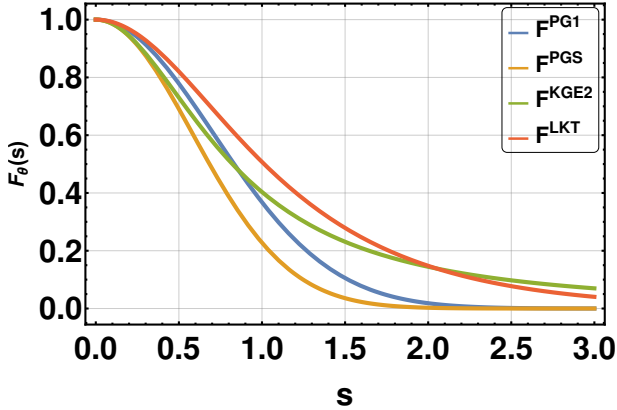


FIG. 1. Plot of Pauli enhancement factors of various functionals as a function of variable s .

We implement a new functional, hereafter referred to as "KGE2":

$$\tau_s = \tau_{TF} \frac{1}{1 + \alpha s^2} + \tau_{vW} \quad (8)$$

$$\text{Where, } s = \frac{|\nabla \rho|}{2k_F \rho} = \frac{|\nabla \rho|}{2(3\pi^2)^{1/3} \rho^{4/3}} = \frac{|\nabla \rho|}{c_s \rho^{4/3}}$$

Where $c_s = 2(3\pi^2)^{1/3}$. Alternatively, τ_s can be expressed as $\tau_s = \tau_{TF} [F_\theta + \frac{5}{3} s^2]$, where $F_\theta = \frac{1}{1 + \alpha s^2}$ is our Pauli enhancement factor and $\lambda = 1$ is chosen.

The corresponding Pauli potential is defined as:

$$v_\theta(\mathbf{r}) = \frac{\delta}{\delta \rho(r)} (T_s[\rho] - T_{vW}[\rho])$$

$$v_s = v_\theta + v_{vW}$$

$$v_{vW}(\mathbf{r}) = \frac{1}{8} \left(\frac{(\nabla \rho(\mathbf{r}))^2}{\rho^2(\mathbf{r})} - 2 \frac{\nabla^2 \rho(\mathbf{r})}{\rho(\mathbf{r})} \right)$$

The explicit form of v_θ for a generic semilocal class of T_s^{GGA} as in Eq.6 is given by:

$$v_\theta = \frac{\partial}{\partial \rho} (\tau_{TF} F_\theta) - \nabla \frac{\partial}{\partial (\nabla \rho)} (\tau_{TF} F_\theta) \\ v_\theta^{KGE2}(\mathbf{r}) = \frac{1}{3} \frac{C_{TF} \rho^{2/3}(\mathbf{r})}{(1 + \alpha s^2)^2} [5 + 11\alpha s^2] + \frac{2}{3} \frac{\alpha C_{TF} \rho^{2/3}(\mathbf{r})}{(1 + \alpha s^2)^3} \\ \times \left[-3s^2 + 13\alpha s^4 + \frac{3\nabla^2 \rho(\mathbf{r})}{c_s^2 \rho^{5/3}(\mathbf{r})} \{1 - 9\alpha s^2\} \right] \quad (9)$$

This form satisfies several known exact conditions of the Pauli potential, as discussed in Ref. [47] and elaborated in the following section.

B. Response function analysis of semilocals

The key feature that distinguishes NL-KEDFs from semilocal-KEDFs are the accurate description of linear response [21, 48]. While semilocal KEDFs do reproduce correct linear response, this holds only when exact small- s limit is enforced. The calculation of the linear response for semilocal KEDFs is more intricate than for NL-KEDFs since the conventional definition of response function: $\frac{1}{\chi(\mathbf{r} - \mathbf{r}')} = \frac{\delta^2 T[\rho]}{\delta \rho(\mathbf{r}) \delta \rho(\mathbf{r}')}$ is not directly applicable. Consider a small perturbation in the uniform electron gas (UEG), with density $\rho = \rho_0 + \rho_q e^{i\mathbf{q} \cdot \mathbf{r}}$. At $r = 0$, this leads to $\rho = \rho_0 + \rho_q$, $\nabla \rho = i\mathbf{q} \rho_q$; $\nabla^2 \rho = -q^2 \rho_q$. We derive the response of the GGA-class of functionals in appendix C, starting from the Pauli potential Eq.9,

$$\frac{1}{\chi^{KGE2}} = \frac{\pi^2}{k_F} - \frac{3}{5} \alpha \eta^2 \frac{\rho_q}{\rho_0} + \frac{18}{5} \frac{\pi^2}{k_F} \alpha \eta^2 \left(\frac{\rho_q}{\rho_0} \right) \left(1 - 8 \frac{\rho_q}{\rho_0} \right) \\ - \frac{9}{5} \frac{\pi^2}{k_F} \eta^2 \left(1 + 3 \frac{\alpha q^2}{k_F^2} \left(\frac{\rho_q}{\rho_0} \right)^2 \right) \\ \frac{1}{\chi^{KGE2}} = \frac{\pi^2}{k_F} \left[1 - \frac{9}{5} \alpha \eta^2 + \mathcal{O}(\rho_q) \right] \quad (10)$$

In last step, the linear response is obtained by collecting ρ_q -independent terms. Now the linear response of v_{vW} is known $\frac{1}{\chi^{vW}} = \frac{\pi^2}{k_F} 3\eta^2$, adding which we get the general linear response for GGA-class of functionals:

$$\frac{1}{\chi_{GGA}} = -\frac{\pi^2}{k_F} \left(\frac{9}{5} \alpha \eta^2 - 3\eta^2 - 1 \right) \quad (11)$$

$$\frac{1}{\chi_\theta^{GGA}} = \frac{1}{\chi_{GGA}} - \frac{1}{\chi^{vW}} - \frac{1}{\chi^{TF}} \quad (12)$$

$$(\chi_\theta^{GGA})^{-1} = -\frac{\pi^2}{k_F} \frac{9}{5} \alpha \eta^2 \quad (13)$$

$$G_\theta^{GGA}(\eta) = \frac{\chi^{TF}}{\chi_\theta^{GGA}} = -\frac{9}{5} \alpha \eta^2 \quad (14)$$

The ability of G_θ^{GGA} to reproduce the NL part of Lindhard function depends critically on the choice of the enhancement

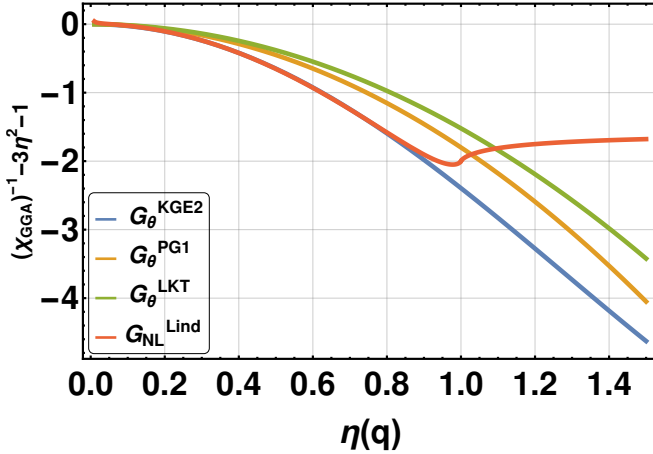


FIG. 2. Here we compare the response function of non-local part of various semilocal KEDFs with exact Lindhard function. The plots are dimensionless as they are normalised with TF response as per Eq.14.

factor. The nonlocal part of Lindhard function is formally defined as: $G_{\text{NL}}^{\text{Lind}} = F^{\text{Lind}} - 3\eta^2 - 1$, where F^{Lind} is the lindhard function [22]. Here we must mention that all the GGA-class of KEDFs and even the mGGA functionals: PGSL and PGSLR has the same form of response function [40] as in Eq.14, only differing by the prefix factor α . This also means that response function of KGE2 and PGS are same in HEG regime. We have plotted all these responses and compared with Lindhard in Fig.2 and showed that adhering by the exact GAE expansion satisfies Lindhard function most accurately, any kind of tuning causes deviation. A similar kind of observation is made regarding quality of density in Sec.III B.

C. Pauli potential and exact constrains

The Pauli potential is perhaps the important aspect in OFDFs, since it is solely responsible for the effects of Pauli-exclusion principle on kinetic part of the energy. In many ways the Pauli potential is similar to XC in DFT, the exact expression of Pauli potential is not known and hence needed to be approximated. Also, the density quality is directly related to Pauli potential [49], and hence, Pauli potential serves as a check on density, which is perhaps the most important quantity in OFDFT.

In early work by Levy (1988) [37, 47], several exact constraints for the Pauli potential were established. These serve as foundational requirements that semilocal functionals often attempt to satisfy, though they are rarely addressed in non-local KEDF formulations. The Pauli potential is defined as:

$$v_\theta = \frac{\delta}{\delta \rho(r)} [T_s - T_{vW}]$$

The Pauli enhancement factor in semi-local functionals highlights that the von Weizsäcker (vW) term alone does not account for the Pauli exclusion principle (PEP). As a result, the atomic or solid-state model in orbital-free density

functional theory (OFDFT) is essentially a fictitious bosonic model, with PEP introduced as a corrective term. This correction is applied through the Pauli potential, denoted by v_{T_θ} . Any bound system must have negative total energy under the presence of external potential, while KE is positive. Again T_{vW} gives us lower bound of the kinetic energy: $T_s \geq T_{vW}$. Hence bringing in the effect of PEP through T_θ will increase the kinetic energy, which gives us one of the important constrain: $T_\theta \geq 0$. In 2011, Nagy [50–52] proposed a method to construct an approximate Pauli potential based on density scaling relations, though further exploration of this approach is needed. One of the standard ways to construct functionals is by use of constrained conditions. Here we present some of them:

- (a) $F_\theta \geq 0$
- (b) $v_\theta(\mathbf{r}) \geq 0$ for all \mathbf{r}
- (c) $t_\theta(\mathbf{r}) \geq 0$ for all \mathbf{r}
- (d) $v_\theta(\mathbf{r}) \geq t_\theta(\mathbf{r})$ for all \mathbf{r}
- (e) $\frac{\tau_\theta[\rho_\lambda]}{\rho_\lambda} = \lambda^2 \frac{\tau_\theta[\rho_\lambda]}{\rho(\lambda\mathbf{r})}$
- (f) $v_\theta[\rho_\lambda](\mathbf{r} = \mathbf{r}_0) = \lambda^2 v_\theta[\rho](\mathbf{r} = \lambda\mathbf{r}_0)$

Here, F_θ is the conventional enhancement factor and T_θ is Pauli energy which is nothing but $T_\theta = T_s - T_{vW} = T_{TF} + T_{NL}$. And $t_\theta = t_s - t_{vW} = \frac{\tau_\theta}{\rho}$ is the Pauli-kinetic-energy-density, with $T_s = \int t_s(\mathbf{r}) n(\mathbf{r}) d\mathbf{r}$. And, λ , where $\lambda \in [0, 1]$ is the scaling parameter (uniform coordinate scaling parameter), that provides insight as to how the functionals behave as the system goes from high to low density and vice versa.

Nevertheless, a good kinetic function, ideally, should satisfy all possible constraints, especially the third and last condition which are based on scaling conditions introduced by Levy and Yang [47] and Pauli positivity. The first two criteria are easily satisfied by observing Eq.7, the third constrain can also be argued to be true as we have even powers of $s(r)$ and density always remains positive. For any pure functional of density like TF, τ_θ/ρ and v_θ has same form, only when $\nabla\rho, \nabla^2\rho$ are involved they differ. Our proposed functional in $s \rightarrow 0$ limit becomes GE of second order, thus inherently satisfying all the scaling conditions. It can also be seen that the quantity s under scaling behaves as $s(\rho_\lambda) \rightarrow s(\lambda)$ which means

$$\begin{aligned} \frac{\tau_\theta^{\text{KGE2}}}{\rho}[\rho_\lambda] &= \lambda^2 C_{TF} \frac{\rho^{2/3}(\lambda\mathbf{r})}{1 + \alpha s^2(\lambda\mathbf{r})} \\ \frac{\tau_\theta^{\text{KGE2}}}{\rho}[\rho_\lambda](r = r_0) &= \lambda^2 \frac{\tau_\theta^{\text{KGE2}}}{\rho}[\rho](r = \lambda r_0) \end{aligned} \quad (15)$$

Similarly one can show that,

$$v_\theta^{\text{KGE2}}[\rho_\lambda](r = r_0) = \lambda^2 v_\theta^{\text{KGE2}}[\rho](r = \lambda r_0) \quad (16)$$

for more details see Appendix.B 1. Apart from these, one can also try and check Lieb-Simon scaling behaviour [53, 54] which is a much more stringent criteria.

III. RESULTS AND DISCUSSIONS

A. Computational Details and Materials

All the OFDFT calculations are done using the DFTpy software package [55]. The KS results for solids are taken from various available literature [20, 42]. We have used LDA level bulk-derived local pseudopotential(BLPS) [55, 56] of Huang and Carter, and we expect the trend of our results to be independent of the choice of pseudopotential as observed in analysis [39] of semilocal KEDFs. We have used the LSDA exchange-correlation [57] in all our calculations. We have chosen a universal parameter for HC ($\lambda = 0.01177$, $\alpha = 1.952$ and $\beta = 0.7143$) [44], $a = 1.3$ for LKT [37], $\mu = 1.0$ for PG1 and $\mu = 40/27$ for PGS [40] in all the calculations for consistency. In this work, all OF-DFT calculations were performed using a kinetic energy cutoff of 1200 eV

For the benchmark calculations of metals, we consider simple metals: Al, Li, and Mg, each with body-centred cubic (BCC), face-centred cubic (FCC), and simple-cubic (SC) phases. For semiconductors, we use nine III-V cubic zincblende (ZB) semiconductors. We compute the equilibrium volume (V_0), bulk moduli (B_0), and equilibrium total energies of all those aforementioned systems. We use the Birch-Murnaghan first-order equation of state [58] to fit the energy versus volume curve.

For calculation of cluster systems, we have considered: Mg8, Mg30, Mg50, Li8, Li30, Al8, Si8, Si30, Al4P4, Al4Sb4, Ga4As4, Ga10As10, Ga4P4, Ga4Sb4, In4As4, In4P4 and In4Sb4. Some of the structures are provided in supporting information [59]. All the rest of the cluster structures are generated by CALYPSO-5.0 code [60–62] with VASP [63] interface. The isolated cluster is placed into an orthorhombic box where the periodic boundary condition is applied. The separations between the studied cluster and its nearest neighboring periodic images are all 16 Å which is large enough to ensure that interactions between the studied cluster and its nearest-neighboring images are negligible. We have selected the most stable structure and performed KS and OFDFT calculation on it.

In generation of these structures the minimal and maximum interatomic distances ranges between 0.7 Å to 2.8 Å appropriately for all cluster systems. To compare the electron densities obtained from different functionals and KS-DFT results, all the electron densities are interpolated on (100,100,100) mesh grids for analysis. The benchmark KS-DFT calculations are carried out with Quantum-ESPRESSO (QE) [64] and 30 Ry energy cutoff are adopted for well-converged total energies 1meV/atom in the same simulation cell as the OF-DFT simulations.

B. Analysis of density

The accuracy of the electron density is as important as, if not more important than, the prediction of total energies. A reliable kinetic energy functional should improve both simultaneously [21]. It is well known that one of the advantages of

nonlocal (NL) KEDFs is their improved accuracy in predicting the density compared to semilocal functionals. As seen in Fig. 3, both KGE2 and PG yield significantly improved densities relative to the Thomas-Fermi-von Weizsäcker (TFvW).

The interstitial region is particularly important, as it represents the bonding region among atoms. This is also where long-range effects or low-momentum ($q \rightarrow 0$) become relevant, the vW term vanishes due to flat density, and the accuracy of the enhancement factor is most critical. Among NL-KEDFs with correct low- q behavior, the jellium-with-gap (JGM) functional [22] and the Huang and Carter (HC) functional [42] are notable. Comparing our results with Kohn-Sham (KS) and HC densities, we find that semilocal KEDFs tend to overestimate the density in regions far from the nucleus.

In the original work on the Pauli-Gaussian (PG) functional [39], the optimized value $\mu = 1$ was identified as yielding the best overall performance. However, we find that $\mu = 40/27$ results in better agreement with KS densities. In fact, any semilocal KEDF that recovers the exact gradient expansion approximation (GEA) consistently produces better density predictions than versions tuned by fitting parameters. Even the addition of meta-GGA corrections, as in PGSL and PGSLr [40], degrades density quality in interstitial regions when compared to PGS and KGE2 (see Fig. 2 in Ref. [59]). This suggests that the inclusion of higher-order terms can worsen the local density description, due to parameter choices optimized for either metals or semiconductors, but not both.

For metallic systems, LKT yields the smallest density errors, followed by KGE2 and then PG1, as shown in Fig. 4. For comparison, we also present the 3D density difference for crystalline silicon in Fig. 5, which reflects similar trends and reinforces our conclusions.

The consistent overestimation of density in interstitial regions suggests a fundamental limitation of the semilocal class of functionals. These regions are characterized by low and relatively uniform densities, where the vW term contributes little and the Pauli term dominates. This implies that the Pauli potential in GGA-level KEDFs may be underestimated in these areas likely due to a TF component that decays too rapidly (see Fig. 3 in Ref. [59]).

A more stringent test for density quality is the density error metric D_0 , defined as:

$$D_0 = \frac{1}{N_e} \int |\rho^{\text{OFDFT}}(\mathbf{r}) - \rho^{\text{KSDF}}(\mathbf{r})| d^3\mathbf{r}, \quad (17)$$

where N_e is the total number of electrons per unit cell. This metric quantifies the overlap between OFDFT and KS densities. The D_0 values for all systems are provided in Table IV of the Supporting Information [59] and summarized in Fig. 6 for clarity.

In general, density errors for semiconductors are approximately twice as large as for metals. Among semilocal functionals, PGS performs best for semiconductors with a mean absolute relative error (MARE) of 16.23%, followed by KGE2 (16.93%) and LKT (18.63%). For comparison, HC achieves a MARE of 11.48%. In metals, LKT again performs best (2.95%), followed by KGE2 (4.75%) and PGS (7.15%). Thus,

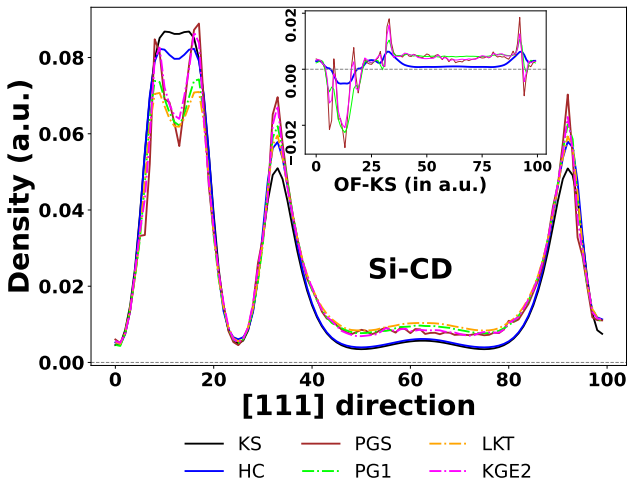


FIG. 3. Density plotting of Si CD along [111] direction for various available KEDFs. The blue line is KS-density; see legend for other labels. The inset plot is density difference $\rho^{KS} - \rho^{OF}$ along [111] direction. The density is in atomic units, and on the x-axis, we have grid points.

PGS shows nearly double the error of its competitors in metals.

Although the mGGA functionals, particularly PGSLr, improve density predictions for metals, their performance is comparable to LKT and consistent with results using PBE exchange-correlation in earlier studies. For semiconductors, however, PGSL and PGSLr show little improvement and remain comparable to PGS and KGE2 despite the addition of two tuning parameters. We observed similar behavior when adding mGGA terms to KGE2 and LKT: while accuracy improved slightly, it required tuning coefficients and violated exact GEA constraints. Since this undermines the primary goal of a simple, parameter-free functional, we do not pursue such modifications in this work.

PGSLr was specifically constructed to preserve the jellium response while incorporating parameter tuning. We argue that rather than introducing additional empirical terms, future improvements should focus on refining the semilocal description within the GGA framework.

C. Assessment of Bulk Properties Using RMARE

The accuracy of a kinetic energy density functional (KEDF) is typically evaluated based on its ability to reproduce both global and local properties. Global properties include structural and mechanical quantities such as equilibrium energy (E_0), bulk modulus (B_0), and equilibrium volume (V_0), while local properties are reflected in the accuracy of the density, potential, and kinetic energy density. In this work, we assess these aspects through four metrics: V_0 , E_0 , B_0 , and the density error (D_0).

To systematically compare functional performance, we adopt the relative median absolute relative error (RMARE),

as introduced in Ref. [39]. The RMARE is defined as:

$$\text{RMARE} = \sum_i \frac{\text{MARE}_i}{\frac{1}{2}(\text{MARE}_i^{HC} + \text{MARE}_i^{SM})} \quad (18)$$

where $i \in \{V_0, E_0, B_0, D_0\}$ and MARE denotes the median absolute relative error. Each component is normalized against the average of the corresponding errors from two benchmark functionals: HC (optimized for semiconductors) and Smargiassi-Madden (SM) [16] (best for metals). To ensure a balanced evaluation, we include ten semiconductors and nine metals in our dataset. Data for V_0 , E_0 , and B_0 for HC and SM are sourced from Refs. [20, 42], while D_0 is computed using fixed parameters $\lambda = 0.01177$ and $\beta = 1.95$. SM is used with its standard internal parameter $A = 0.2$.

Figure 6 and Table I summarize the RMARE statistics for each functional. The box plots illustrate the distribution of errors, with quartiles ($Q1$ and $Q3$) defining the box boundaries, whiskers extending to non-outlier extrema, and outliers marked individually. The yellow band indicates the median error, while the box height reflects the spread, serving as a visual proxy for standard deviation.

We benchmark KGE2 against several semilocal and mGGA-level functionals, as well as the nonlocal HC functional. As discussed in Sec. III B, we focus here on structural properties. Among semilocal GGA-level functionals, KGE2 exhibits the best overall performance, achieving the lowest RMARE (5.82%), outperforming PG1 (7.40%), PGS, and LKT. Even the mGGA extensions of PG-class functionals fail to surpass KGE2 in accuracy, despite their higher computational cost. This result supports our goal of constructing a parameter-free, generally accurate, and computationally efficient KEDF.

For semiconductors, PGS yields the most accurate equilibrium energy (E_0) and the best D_0 among semilocal functionals, with an RMARE of 3.71%. However, its performance on V_0 and B_0 is less satisfactory. PG1, constructed by tuning the μ parameter, improves V_0 and B_0 but worsens E_0 and D_0 , raising the overall RMARE to 7.51%. This highlights the drawbacks of parameter tuning, which KGE2 avoids by construction. With an RMARE of 4.47%, KGE2 outperforms even PGS and PGSLr, the latter of which includes mGGA terms. The relatively poor performance of PGSLr in semiconductors suggests that its parameters ($\beta = 0.25$, $\lambda = 0.4$, $\sigma = 0.2$) deviate from optimal behavior for localized systems. LKT performs the worst in this category, despite relatively stable values for V_0 and B_0 across both material types.

In contrast, the trend reverses for metals. Here, LKT performs best among all semilocal and mGGA functionals, with an RMARE of 7.24%, followed by PGSLr and PGSL. KGE2 performs comparatively poorly, while PGS shows the highest error, nearly four times that of LKT. The addition of mGGA terms in PGSLr improves both structural and density predictions for metals, suggesting that it better captures metallic response behavior. The sharp decline of the enhancement factor $F_\theta(s)$ in PG at large s effectively suppresses the TF component, leading to an overemphasis on the vW term, a behavior akin to a bosonic system. This imbalance can be corrected either by reducing the steepness of the slope ($\mu : 1.48 \rightarrow 1.0$)

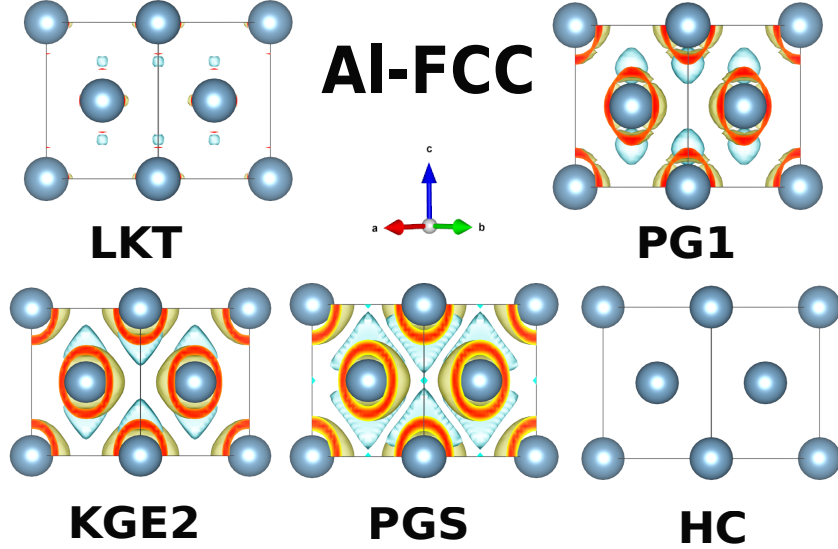


FIG. 4. Density difference of Al-FCC (KS-OF) in 3D in the order: TFvW, PG , KGE2 and LKT. We have chosen this view to display how the density improves with increasing functional quality. Isoscale is set at 100% yellow saturation for density difference of 0.02 $a.u$ and 100% blue saturation for density difference -0.02 $a.u$..

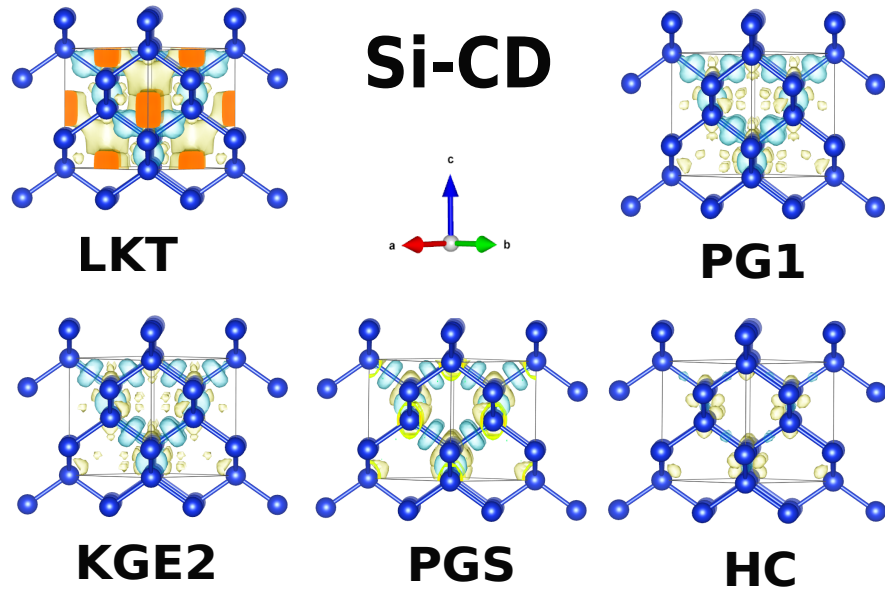


FIG. 5. Density difference of Si-CD (KS-OF) in 3D in the order: WT, TFvW, LKT, PG, KGE2 and HC. We have chosen this view to display how the density improves with increasing functional quality. Isoscale is set at 100% yellow saturation for density difference of 0.035 $a.u$ and 100% blue saturation for density difference -0.035 $a.u$..

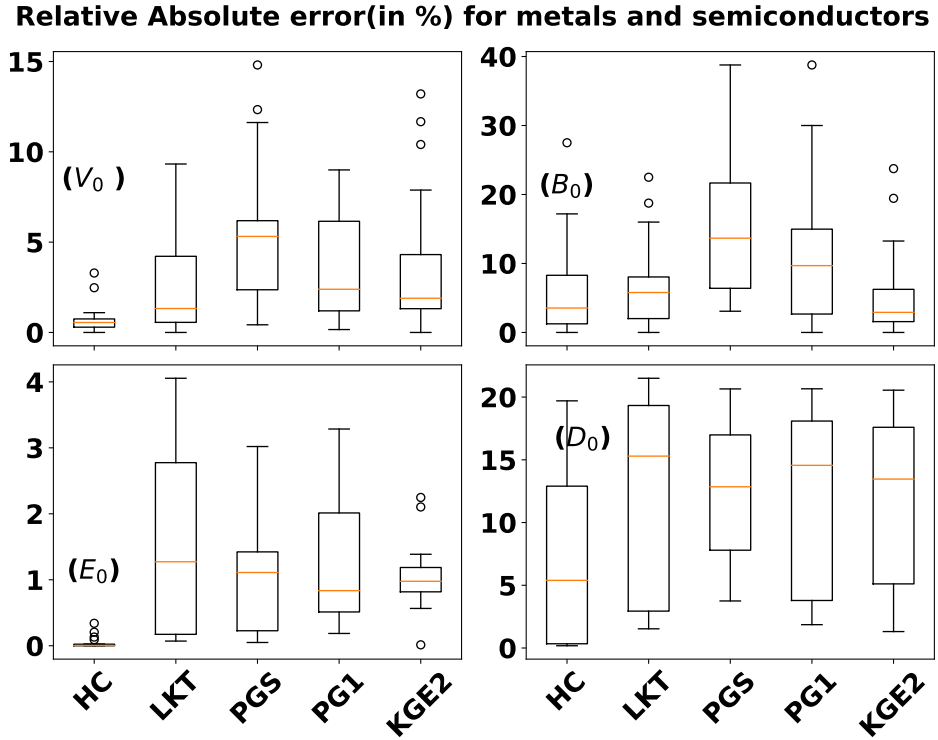


FIG. 6. Box plot of relative absolute error (in %) of equilibrium volume (V_0), bulk modulus(B_0), energy(E_0) and density error (D_0) for semiconductors and metals. The box plot used here summarizes the overall distribution of a set of data points in Table.1, Table.2, Table.3 and Table.5 of supporting information [59].

TABLE I. Relative median absolute error (RMARE) in (%) of various functionals on Solids. The boldface values represent the best values in semilocal level.

	SM ($A = 0.2$) ($\lambda = 0.011$) ($\beta = 0.71$)	HC ($a = 1.3$)	LKT ($a = 1.3$)	PGS ($\mu = 1.48$)	PG1 ($\mu = 1$)	KGE2 ($\alpha = 1.48$)	PGSL ($\beta = 0.25$)	PGSLr ($\lambda = 0.4$) ($\sigma = 0.2$)
RMARE (semi+metal)	6.825	1.174	6.984	7.771	7.40	5.822	6.984	6.370
RMARE (semi)	6.738	1.261	8.723	3.719	7.515	4.469	6.315	5.539
RMARE (metals)	5.808	2.191	7.241	27.075	11.992	17.976	9.749	7.840

or by incorporating mGGA terms to compensate. This rationale also explains why the GE4 coefficient $\beta = 8/81$ is increased to $\beta = 1/4$ in PGSL-type functionals. PGSLr also benefits from a well-behaved response function, as illustrated in Fig. 3 of Ref. [39]. However, the increased parameter count and higher computational cost, along with poor convergence behavior, especially for finite systems, limit their practicality as general-purpose OF-KEDFs.

For detailed MARE values separated by semiconductors and metals, refer to the Supporting Information [59]. From this analysis, we conclude that metallic systems benefit from a slowly decaying $F_\theta(s)$ in the low- s regime, whereas semiconductors perform better when $F_\theta(s)$ decays rapidly at high s . The transition point for this change in behavior is system-specific. In practice, tuning parameters in enhancement factors indirectly controls this inflection point. Ideally, a semilocal KEDF would treat this crossover as a spatially varying, nonlocal feature, modulating the TF contribution based on the

local environment.

D. Elastic Properties

A precise description of the response function is essential for the construction of a high-quality kinetic energy density functional (KEDF) [65]. Mechanical properties, in particular, provide a stringent test of a KEDF's performance, as they are directly linked to the system's linear response behavior [66, 67]. When a lattice is deformed, the external potential is perturbed, which induces changes in the electron density. A reliable KEDF must correctly reproduce the resulting stress response through its dependence on the density.

The relationship between stress (σ) and strain (ε) is given by $\sigma_j = \sum_i C_{ij} \varepsilon_j$, where C_{ij} is the elastic stiffness tensor [29].

For cubic crystals, symmetry reduces the number of independent components to three: C_{11} , C_{12} , and C_{44} . We compute

TABLE II. Bulk modulus (B), C_{11} , C_{12} and triaxial shear modulus (C_{44}) for CD Si calculated by KSDFT and OFDFT with the HC and the current semi local KEDFs. For HC and KGAP we have used optimal choices of the parameters mentioned in [20, 42] respectively. (* denotes unstable structure.) Same parameters are used for HC, PG1 and KGE2 as mentioned in computational details Sec. III A.

elements	Functional	C_{11} (GPa)	C_{12} (GPa)	C_{44} (GPa)
Si-CD	KS ([67])	162	65	76
	HC	101	92	81
	KGAP *	46	98	77
	TFvW *	23	142	77
	KGE2 *	58	122	35
	PG1 *	2	301	-142
GaP	KS	141	67	67
	HC *	12	89	-39
	KGE2	96	31	19
	PG1	349	-4	54
GaSb	KS	86	40	41
	HC	51	49	43
	KGE2	20	63	26
	PG1 *	248	58	-44
InAs	KS	84	49	36
	HC *	34	44	22
	KGE2	29	61	79
	PG1 *	-176	131	120
InP	KS	99	58	42
	HC *	31	94	37
	KGE2	132	60	92
	PG1	1719	86	1051

C_{44} by applying a triaxial shear strain $\varepsilon = (0, 0, 0, \delta, \delta, \delta)$, and C_{11} and C_{12} using a biaxial strain $\varepsilon = (\delta, \delta, 0, 0, 0, 0)$. The bulk modulus B_0 is obtained via $B_0 = (C_{11} + 2C_{12})/3$, while C_{44} is extracted from the strain energy relation: $\Delta E/V_0 = \frac{3}{2}C_{44}\delta^2$.

A robust KEDF should also satisfy the mechanical stability criteria for cubic systems:

1. $C_{11} - C_{12} > 0$,
2. $C_{11} + 2C_{12} > 0$,
3. $C_{44} > 0$.

These conditions are stringent and often not satisfied, even by advanced nonlocal functionals. While all the materials studied here meet these criteria, suggesting room for improvement in OF-KEDFs, our proposed semilocal functional, KGE2, performs competitively with complex NL-KEDFs such as HC and JGM. Despite structural similarities between PG1 and KGE2, PG1 yields substantial errors in elastic constants, while TFvW performs the worst across all metrics.

Huang and Carter previously reported [67] that the WGC-class functional fails to accurately predict elastic constants for the Si-CD phase. Among the semilocal functionals we tested, only PG1 and KGE2 correctly predict the stability of GaP, GaSb, InAs, and InP. In contrast, MGP fails to capture the elastic tensor accurately, often producing negative C_{11} and C_{12} values. Other functionals, including WT, SM, and TFvW, also perform poorly in this regard.

E. Application of KGE2 on finite systems: Clusters

To assess KEDF performance on finite systems, we examine four key metrics: (1) electron density, (2) Pauli potential, (3) kinetic energy density, and (4) total energy. Results for these quantities are presented in Figs. 7, 8, and 9. Although absolute total energies suffer from significant error cancellation among Hamiltonian components and thus carry limited physical weight, we include them for completeness and direct comparison. We limit our study of semilocal KEDFs to the GGA level because mGGA terms often amplify numerical noise in low-density regions, leading to difficulties in convergence in PAW based codes like DFTPy. In existing semilocal functionals, the mGGA contribution serves primarily as a corrective term atop the GGA baseline, which accounts for the bulk of the kinetic energy. Accordingly, we concentrate here on constructing an accurate GGA component, with the understanding that the subsequent inclusion of mGGA corrections would further refine the density description. Finite systems, particularly isolated atoms, are especially valuable test cases because they eliminate spurious density overlap and thereby clarify functional behaviour.

For global error indicator we have modified the definition of RMARE from Eq.18 as :

$$\text{RMARE} = \sum_i \frac{\text{MARE}_i}{\frac{1}{2}[\text{MARE}_i^{\text{HC}} + \text{MARE}_i^{\text{LMGP}}]} \quad (19)$$

where $i \in \{\Delta E, D_0\}$ with ΔE are same as defined in Sec. III C. We have taken 18 cluster systems: as mentioned in Sec. III A.

The information of structure of clusters are given in Sec. III A. In Fig. 7 we have plotted a Boxplot of the relative absolute error of energy and density, just as in Fig. 6, refer to the caption for details of the Boxplot. The description of Boxplot here remains same as explained in Sec. III C. We have chosen to benchmark KGE2 with TFvW, PGS and LKT and with best NL-KEDFs: HC with universal parameters and LMGP fixed at it's internally optimized parameter $A=0.2$. In Table. III we also report RMARE for various semilocal and nonlocal KEDFs which again asserts our claim that performance of KGE2 is balanced between PGS and LKT. However we note that among all semilocals the TFvW performs poorly in describing energy and density when compared with advanced GGA-KEDFs. It should be noted that we PG1 has performed poor for clusters perhaps because $\mu = 1$ was optimized for solids, whereas PGS has performed well for atoms as was observed in [41].

Regarding the non-local Pauli functionals, it has been discussed in [68] that the Pauli positivity condition is violated for most NL-class of approximations in low density $n(\mathbf{r}) \rightarrow 0$ regime. One may also note that the scaling (λ) relation is violated by WT NL-functionals as discussed in [68]. However, these problems are not faced by semilocal-class of functionals, as all the constraints on Pauli potential discussed in Sec. II C are theoretically satisfied, but PG-class fails to satisfy these in some instances due to numerical noise. We have also shown in Fig.8 that almost all the KEDFs satisfy the Pauli positivity condition with PGS in Fig. 9 as an exception due to high numerical noise. From the Pauli potential of He-atom, it is clear

TABLE III. Relative Mean Absolute Relative Errors (RMAREs) of various functionals when applied on clusters.

Functional	TFvW	LMGP ($A = 0.2$)	HC ($\lambda = 0.01177$)	LKT	KGE2	PGS
RMARE	11.10	2.33	1.66	5.12	4.76	3.64

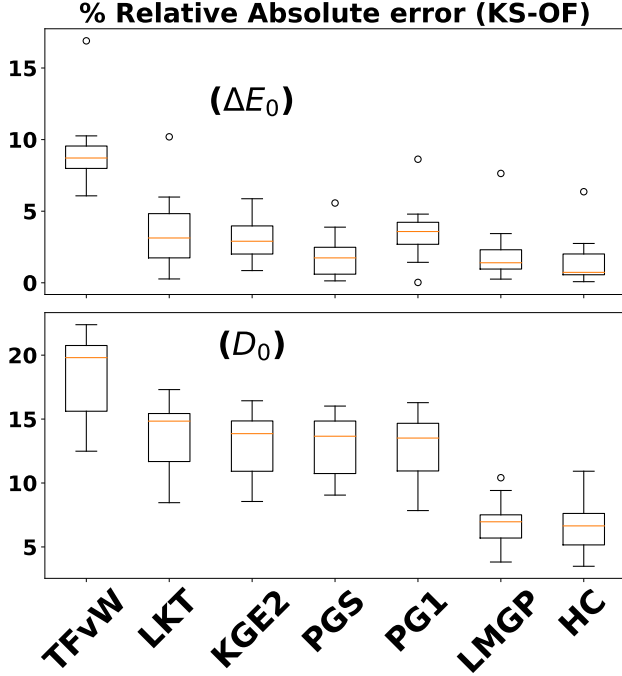


FIG. 7. Boxplot of absolute error of energy(E_0) in eV and Density-error plot (D_0). The Boxplot used here summarizes the overall distribution of a set of data points in Table.VI and Table.VII of supporting information[59].

that none of the OF-KEDFS could give vanishing Pauli potential, except KGE2, which majorly remains at the zero level, however, has an unexpected bump away from the nucleus.

The violation of constrain-(c): $v_{T_\theta}[n](\mathbf{r}) \geq \frac{t_\theta[n](\mathbf{r})}{n(\mathbf{r})}$, in near nucleus region is a major indicator that showcases the drawback of simplistic description of semilocals which on the other hand nonlocals satisfy with ease. It is also interesting to notice how, in the long range, the fall of the Pauli potential is slower than all the semilocals. And just after the plateau region, all the semilocals converge with HC. This brings us to the question how should be the exact decay rate of Pauli potential, and in the work of [41, 47], for spherical-symmetry atoms the Pauli potential in the tailing end decays as $\frac{1}{r^2}$, in fact, the exact expression given as: $v_\theta \rightarrow \frac{l(l+1)}{2} \frac{1}{r^2}$; where l is the azimuthal quantum number. This decay rate is obeyed by almost all of the functionals correctly when away from the nucleus.

We report the mean of absolute error (MAE) in energy of about 1.15 eV for PGS, which is about 1.74% error (MARE) is the least error followed by KGE2 and LKT, respectively, with percentage errors 3.15% and 3.42% in Fig. 7. And with a relative error in density of 12.89% for PGS, 13.19% for KGE2

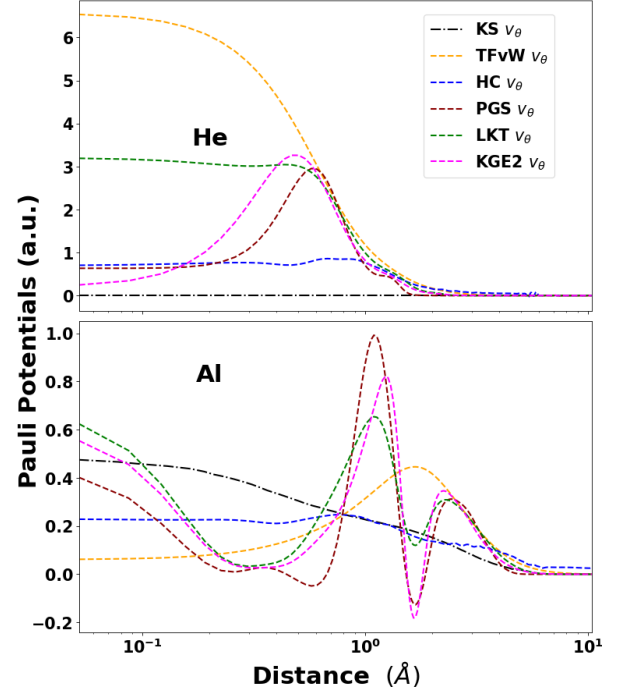


FIG. 8. Numerical Pauli potential for He atom (upper panel) and Al atom (lower panel)

and 13.65% for LKT. Of course, the density-dependent nonlocal kernels like HC and LMGP outperform all the semilocals by a large margin. Note that this error in energy might seem huge as compared to bulk systems where the % error of energy of HC is typically 0.46% and 8.3% for energy and density respectively (see table.1 of [39]). This systematic large MARE for the local system is due to the presence of a large vacuum present in the simulation box [69], and we have also found this vacuum responsible for the slow convergence of many semilocal functionals (especially PG-class).

Though the pure non-empirical nature of semilocal as compared to nonlocals gives an extra edge for the predictability of unknown materials, however, the Pauli potential of all the semilocals behaves similarly and poorly. We believe that the uncontrollable oscillation of the Pauli potential for all the semilocal KEDFs hints towards some major drawback, resolving which can result in better accuracy of one-point kinetic energy functionals in general.

IV. CONCLUSION

We have proposed a semilocal kinetic energy density functional (KGE2), constructed from first principles with-

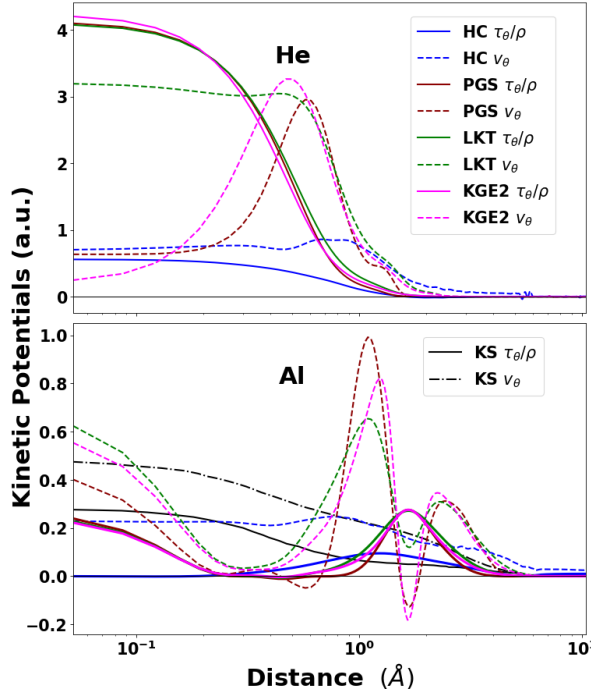


FIG. 9. Numerical kinetic energy density for He atom (upper panel) and Al atom (lower panel).

out any tunable parameters. It achieves a level of accuracy that competes with state-of-the-art nonlocal and meta-GGA functionals, while remaining computationally efficient. The functional reintroduces the Thomas–Fermi–von Weizsäcker (TFvW) framework with a refined balance between the TF and vW contributions, respecting the exact second-order gradient expansion.

Our benchmarks demonstrate that KGE2 performs comparably to nonlocal KEDFs in predicting structural and mechanical properties of both metals and semiconductors. Among semilocal functionals, KGE2 consistently yields balanced accuracy across materials classes outperforming PG-class for metals and LKT for semiconductors. Although meta-GGA-level functionals like PGSL and PGSLr show significantly good results for specific material types, they involve parameter fitting and incur higher computational cost. In contrast, KGE2 maintains parameter-free construction and still surpasses PGSL and PGSLr in average performance for solids. For finite systems, especially small clusters, nonlocal functionals still outperform semilocal ones by a significant margin, though the performance gap narrows with increasing cluster size. Though semilocal KEDFs satisfy all the Pauli constraints by construction, we have showed that some important constraints do fail numerically. Investigating these could bring new insights to drawbacks of semilocal class of functionals.

Overall, KGE2 provides a physically motivated, simple, computationally inexpensive, and parameter-free KEDF that delivers reliable performance across both bulk and finite systems. Its balanced accuracy and simplicity make it a strong candidate for general-purpose orbital-free DFT applications

in metals and semiconductors alike.

DATA AVAILABILITY

The data supporting the findings of this article are available freely in supplementary materials [59]. The geometry files of all the structures and modified version of DFTpy with KGE2 implemented will be provided upon request.

ACKNOWLEDGMENTS

The authors acknowledge partial financial and computational support from the National Institute of Science Education and Research (NISER). The author thanks physics department of IIT Kanpur for partial fundings and

Appendix A: Pauli Potential of semilocals:

Any generic semilocal functional can be written in the following form:

$$T_\theta = \int d\mathbf{r} \tau_{TF}(\rho) F_\theta(s)$$

And the Pauli potential as defined in Sec.I,

$$\begin{aligned} v_\theta(\mathbf{r}) &= \frac{\delta}{\delta \rho(\mathbf{r}')} \int d\mathbf{r} \tau_{TF}(\rho) F_\theta(s) \\ &= \frac{\partial}{\partial \rho} (\tau_{TF} F_\theta) - \nabla \frac{\partial}{\partial (\nabla \rho)} (\tau_{TF} F_\theta) \\ &= \frac{5}{3} C_{TF} \rho^{2/3} F_\theta(s) + C_{TF} \rho^{5/3} \frac{\partial F_\theta}{\partial \rho} - \nabla \left[\tau_{TF} \frac{\partial F_\theta}{\partial (\nabla \rho)} \right] \\ &= \frac{5}{3} C_{TF} \rho^{2/3} F_\theta + C_{TF} \rho^{5/3} \frac{\partial F_\theta}{\partial s} \cdot \frac{\partial s}{\partial \rho} - \nabla \left[C_{TF} \rho^{5/3} \frac{\partial F_\theta}{\partial s} \frac{\partial s}{\partial \rho} \right] \\ v_\theta(r) &= \frac{5}{3} C_{TF} \rho^{2/3} F_\theta(s) - \frac{4}{3} C_{TF} \rho^{2/3} s \left(\frac{\partial F_\theta}{\partial s} \right) - \frac{C_{TF}}{c_s} \nabla \left[\rho^{1/3} \frac{\partial F_\theta}{\partial s} \right] \end{aligned} \quad (\text{A1})$$

where we have used, $\frac{\partial F_\theta}{\partial \rho} = \frac{\partial F_\theta}{\partial s} \cdot \frac{\partial s}{\partial \rho} = -\frac{4}{3} \frac{s}{\rho} \cdot \frac{\partial F_\theta}{\partial s}$ and $\frac{\partial F_\theta}{\partial (\nabla \rho)} = \frac{1}{c_s \rho^{4/3}} \cdot \frac{\partial F_\theta}{\partial s}$,

We can see that putting $F_\theta = 1$ readily gives us TF potential. Now plugging the form of Eq.7 we get

$$\begin{aligned} v_{\text{KGE2}}(\mathbf{r}) &= \frac{1}{3} \frac{C_{TF} \rho^{2/3}(\mathbf{r})}{(1 + \alpha s^2)^2} [5 + 11\alpha s^2] + \frac{2}{3} \frac{\alpha C_{TF} \rho^{2/3}(\mathbf{r})}{(1 + \alpha s^2)^3} \\ &\quad \times \left[-3s^2 + 13\alpha s^4 + \frac{3\nabla^2 \rho(\mathbf{r})}{c_s^2 \rho^{5/3}(\mathbf{r})} \{1 - 9\alpha s^2\} \right] \end{aligned} \quad (\text{A2})$$

Appendix B: Exact conditions of v_θ

1. Scaling conditions

Here we show how scaling condition is satisfied by KGE2 functional. The scaling conditions are given by:

$$v_\theta[\rho_\lambda](\mathbf{r} = \mathbf{r}_0) = \lambda^2 v_\theta[\rho](\mathbf{r} = \lambda \mathbf{r})$$

where $\rho_\lambda = \lambda^3 \rho(\lambda \mathbf{r})$.

$$v_\theta(\mathbf{r}) = \frac{1}{3} \frac{C_{TF} \rho^{2/3}(\mathbf{r})}{(1 + \alpha s^2)^2} [5 + 11\alpha s^2] + \frac{2}{3} \frac{\alpha C_{TF} \rho^{2/3}(\mathbf{r})}{(1 + \alpha s^2)^3} \times \left[-3s^2 + 13\alpha s^4 + \frac{3\nabla^2 \rho(\mathbf{r})}{c_s^2 \rho^{5/3}(\mathbf{r})} \{1 - 9\alpha s^2\} \right]$$

Let's check how $s(\rho, \nabla \rho)$ behaves under this scaling.

$$\begin{aligned} s(\rho_\lambda) &= \frac{\nabla(\lambda^3 \rho(\lambda \mathbf{r}))}{c_s \lambda^4 \rho^{4/3}(\lambda \mathbf{r})} \\ &= \frac{\nabla_\lambda \rho(\lambda \mathbf{r})}{c_s \rho_\lambda^{4/3}(\mathbf{r})} = s(\lambda \mathbf{r}) \end{aligned}$$

$$\text{Thus, } s(\rho_\lambda) \rightarrow s(\lambda \mathbf{r}); \quad s^2(\rho_\lambda) \rightarrow s^2(\lambda \mathbf{r}) \quad (\text{B1})$$

Similarly it can be shown that, $\frac{\nabla^2 \rho(\mathbf{r})}{\rho^{5/3}(\mathbf{r})} \rightarrow \frac{\nabla^2 \rho(\lambda \mathbf{r})}{\rho^{5/3}(\lambda \mathbf{r})}$. Using these it can be shown that,

$$v_\theta^{KGE2}[\rho_\lambda](r = r_0) = \lambda^2 v_\theta^{KGE2}[\rho](r = \lambda r_0) \quad (\text{B2})$$

Appendix C: Response function for GGA functionals

1. Method 1: Perturbing the kinetic potential

The following steps are taken in order :

- Calculate (kinetic)potential from KE expression.
- Perturb the the density arround $r=0$, and plug in potential.
- Take functional derivative.

Consider a small perturbation in the uniform electron gas (UEG) density, $k_F = (3\pi^2 \rho_0)^{1/3}$, $\rho = \rho_0 + \rho_q e^{iq \cdot r}$ at $r = 0$ we get $\rho = \rho_0 + \rho_q$, $\nabla \rho = iq \rho_q$; $\nabla^2 \rho = -q^2 \rho_q$, which implies:

$$s = \frac{1}{2(3\pi^2)^{1/3}} \frac{iq \rho_q}{(\rho_0 + \rho_q)^{4/3}} \quad (\text{C1})$$

a. Response of vW Functional:

$$\begin{aligned} T^{vW} &= \int \frac{1}{8} \frac{|\nabla \rho|^2}{\rho} dr; \\ v^{vW} &= -\frac{1}{8} \frac{(\nabla \rho)^2}{\rho^2} + \frac{1}{4} \frac{\nabla^2 \rho}{\rho} = \frac{q^2}{8} \left(2 \frac{\rho_q^2}{\rho^2} - 2 \frac{1}{\rho} \right) \quad (\text{C2}) \end{aligned}$$

Now we take the limit $\rho_0 \gg \rho_q$ and $\delta \rho = \rho_q \rightarrow 0$ for small perturbation.

$$\begin{aligned} \frac{\delta v^{vW}}{\delta \rho} &= \frac{\delta v^{vW}}{\delta \rho_q} = -\frac{q^2}{4\rho_0}; \\ \frac{1}{\chi^{vW}} &= \frac{\pi^2}{k_F} 3\eta^2 \end{aligned} \quad (\text{C3})$$

In the last step we have used the following: $\rho_0 = \frac{k_F^3}{3\pi^2}$, $\eta = \frac{q}{2k_F}$

b. Response of KGE2 functional:

$$\begin{aligned} v_\theta^{KGE2}(\mathbf{r}) &= \frac{1}{3} \frac{C_{TF} \rho^{2/3}(\mathbf{r})}{(1 + \alpha s^2)^2} [5 + 11\alpha s^2] + \frac{2}{3} \frac{\alpha C_{TF} \rho^{2/3}(\mathbf{r})}{(1 + \alpha s^2)^3} \\ &\quad \times \left[-3s^2 + 13\alpha s^4 + \frac{3\nabla^2 \rho(\mathbf{r})}{c_s^2 \rho^{5/3}(\mathbf{r})} \{1 - 9\alpha s^2\} \right] \end{aligned}$$

Where $C_{TF} = \frac{3}{10} (3\pi^2)^{2/3}$; $c_s = 2(3\pi^2)^{1/3}$.

Lets work with **first term** ($v_\theta^{KGE2,1}$):

$$\begin{aligned} v_\theta^{KGE2,1} &= \frac{1}{3} C_{TF} \frac{\rho^{2/3}}{(1 + \alpha s^2)^2} \left[1 + \frac{11}{5} \alpha s^2 \right] \\ &\quad \frac{1}{(1 + \alpha s^2)^2} \approx 1 - 2\alpha s + \dots \end{aligned} \quad (\text{C4})$$

$$\begin{aligned} v_\theta^{KGE2,1} &= \frac{5}{3} C_{TF} \rho^{2/3} \frac{1}{(1 + \alpha s^2)} \left[1 - \frac{11}{5} \alpha \frac{4(3\pi^2)^{2/3}}{\rho^{8/3}} \frac{-q^2 \rho_q^2}{\rho^{8/3}} \right] \\ &= \frac{5}{3} C_{TF} \rho^{2/3} \left(1 + 2\alpha' \frac{q^2 \rho_q^2}{\rho^{8/3}} \right) \left(1 - \frac{11}{5} \alpha' \frac{q^2 \rho_q^2}{\rho^{8/3}} + \mathcal{O}(\rho_q^4) \right) \\ &= \frac{5}{3} C_{TF} \rho_0^{2/3} \left(1 - \frac{1}{5} \alpha' \frac{q^2 \rho_q^2}{\rho_0^{8/3}} + \mathcal{O}(\rho_q^3) \right) \end{aligned} \quad (\text{C5})$$

$$\begin{aligned} (\chi^{-1})^{1st} &= \frac{\delta}{\delta \rho} v_1^{KGE2} = \frac{5}{3} C_{TF} \rho_0^{2/3} \left(\frac{2}{3\rho_0^{1/3}} - \frac{6}{5} \frac{\alpha' q^2}{\rho_0^{8/3}} \rho_q \right) \\ &= \frac{\pi^2}{k_F} - \frac{3}{5} \alpha \eta^2 \frac{\rho_q}{\rho_0} \quad \text{where, } \eta = \frac{q}{2k_F} \\ (\chi^{-1})^{1st} &= \chi_{TF}^{-1} - \frac{3}{5} \alpha \eta^2 \frac{\rho_q}{\rho_0} \end{aligned} \quad (\text{C6})$$

Now with **second and third term**:

$$\begin{aligned} v_\theta^{KGE2,2,3} &= \frac{2}{3} C_{TF} \alpha \rho^{2/3} \frac{1}{(1 + \alpha s^2)^3} \{-3s^2 + 13s^4\} \\ &= \frac{2}{3} C_{TF} \alpha \rho^{2/3} (1 - 3\alpha s^2 + \mathcal{O}(s^4)) (-3s^2 + \mathcal{O}(s^4)) \\ &= \frac{2}{3} C_{TF} \alpha \rho_0^{2/3} (-3s^2 + \mathcal{O}(s^4)) \end{aligned}$$

Now, $s^2 \rho_q^2 = -\frac{q^2}{4(3\pi^2)^{2/3}} \frac{\rho_q^4}{\rho_0^{8/3}}$; $\frac{\partial(s^2 \rho_q^2)}{\partial \rho_q} = -\frac{6q^2}{4(3\pi^2)^{2/3}} \frac{\rho_q^3}{\rho_0^{8/3}}$; $\frac{\partial(s^4 \rho_q^2)}{\partial \rho_q} = \frac{6q^4}{(4(3\pi^2))^2} \frac{\rho_q^5}{\rho_0^{16/3}}$. And we discard all the terms of order above $\mathcal{O}(\rho_q^2)$. With these simplifications we have final form putting expression of s^2 :

$$v_\theta^{KGE2,2,3} = \frac{3}{20} \alpha q^2 \left(\frac{\rho_q}{\rho_0} \right)^2 \left(1 - \frac{8}{3} \frac{\rho_k}{\rho_0} \right) \quad (C7)$$

$$\begin{aligned} \frac{\partial v_\theta^{KGE2,2,3}}{\partial \rho_q} &= \frac{3}{20} \alpha q^2 \left(\frac{\rho_q}{\rho_0} \right)^2 \left(1 - \frac{8}{3} \frac{\rho_q^2}{\rho_0} \right) \quad (C8) \\ (\chi^{-1})^{2,3} &= \frac{3}{10} \frac{\alpha q^2}{\rho_0^2} \left[1 - 8 \frac{\rho_k}{\rho_0} \right] \rho_q \\ (\chi^{-1})^{2,3} &= \frac{6}{5} \alpha \frac{(3\pi^2)^{2/3}}{\rho_0^{4/3}} \eta^2 \left[1 - 8 \frac{\rho_q}{\rho_0} \right] \rho_q \end{aligned}$$

Similarly, for **fourth and fifth term**:

$$\begin{aligned} v_\theta^{KGE2,4,5} &= \frac{2}{3} \frac{C_{TF} \alpha \rho^{2/3}}{(1 + \alpha s^2)^3} \left[3 \frac{\nabla^2 \rho}{c_s^2 \rho^{5/3}} (1 - 9\alpha s^2) \right] \\ &\quad \text{Now, } \nabla^2 \rho \ll \nabla \rho; \\ &= 2 \frac{\alpha C_{TF}}{c_s^2 \rho} (1 - 3\alpha s^2) (1 - 9\alpha s^2) \nabla^2 \rho \\ &= -\frac{3}{20} \frac{\alpha}{\rho_0} [1 - 12\alpha s^2 + \mathcal{O}(s^2)] q^2 \rho_k^2 \quad (C9) \end{aligned}$$

Where in the last step we used small perturbation approximations.

$$\begin{aligned} \frac{\partial v_\theta^{KGE2,4,5}}{\partial \rho_q} &= -\frac{3}{20} \frac{\alpha q^2}{\rho_0} \left(1 + 3 \frac{\alpha}{(3\pi^2)^2} q^2 \frac{\rho_q^2}{\rho_0^{8/3}} \right) \\ (\chi^{-1})^{4,5} &= -\frac{3}{20} \frac{\alpha}{\rho_0} 4\eta^2 (3\pi^2 \rho_0)^{2/3} \left[1 + 3 \frac{\alpha q^2}{(3\pi^2 \rho_0)^{2/3}} \left(\frac{\rho_q}{\rho_0} \right)^2 \right] \quad (C10) \end{aligned}$$

where in last step The final expression of χ^{PG} is:

$$\begin{aligned} (\chi^{-1})^{KGE2} &= \frac{\pi^2}{k_F} - \frac{3}{5} \alpha \eta^2 \frac{\rho_q}{\rho_0} + \frac{18}{5} \frac{\pi^2}{k_F} \alpha \eta^2 \left(\frac{\rho_q}{\rho_0} \right) \left(1 - 8 \frac{\rho_q}{\rho_0} \right) \\ &\quad - \frac{9}{5} \frac{\pi^2}{k_F} \eta^2 \left(1 + 3 \frac{\alpha q^2}{k_F^2} \left(\frac{\rho_q}{\rho_0} \right)^2 \right) \quad (C11) \end{aligned}$$

considering low-s limit, if $\delta \rho = \rho_q \rightarrow 0$, we get,

$$\chi^{-1} = \frac{\pi^2}{k_F} \left\{ 1 - \frac{9}{5} \alpha \eta^2 \right\} \quad (C12)$$

putting $\alpha = 0$, we can recover TF response function which is expected.

[1] P. Hohenberg and W. Kohn, Phys. Rev. **136**, B864 (1964), URL <https://link.aps.org/doi/10.1103/PhysRev.136.B864>.

[2] W. Kohn and L. J. Sham, Phys. Rev. **140**, A1133 (1965).

[3] L. H. Thomas, Mathematical Proceedings of the Cambridge Philosophical Society **23**, 542 (1927).

[4] T. Sjostrom and J. Daligault, Phys. Rev. Lett. **113**, 155006 (2014), URL <https://link.aps.org/doi/10.1103/PhysRevLett.113.155006>.

[5] Y. H. Ding, A. J. White, S. X. Hu, O. Certik, and L. A. Collins, Phys. Rev. Lett. **121**, 145001 (2018), URL <https://link.aps.org/doi/10.1103/PhysRevLett.121.145001>.

[6] G. Vignale, Phys. Rev. A **77**, 062511 (2008), URL <https://link.aps.org/doi/10.1103/PhysRevA.77.062511>.

[7] F. Della Sala, The Journal of Chemical Physics **157**, 104101 (2022), URL https://pubs.aip.org/aip/jcp/article-pdf/doi/10.1063/5.0100797/16548825/104101_1_online.pdf, URL <https://doi.org/10.1063/5.0100797>.

[8] K. Jiang and M. Pavanello, Phys. Rev. B **103**, 245102 (2021), URL <https://link.aps.org/doi/10.1103/PhysRevB.103.245102>.

[9] K. Jiang, X. Shao, and M. Pavanello, Phys. Rev. B **104**, 235110 (2021), URL <https://link.aps.org/doi/10.1103/PhysRevB.104.235110>.

[10] J. Aarons, M. Sarwar, D. Thompsett, and C.-K. Skylaris, The Journal of Chemical Physics **145**, 220901 (2016), ISSN 0021-9606, URL https://pubs.aip.org/aip/jcp/article-pdf/doi/10.1063/1.4972007/15519363/220901_1_online.pdf, URL <https://doi.org/10.1063/1.4972007>.

[11] R. G. Parr and W. Yang, *Density-Functional Theory of Atoms and Molecules* (Oxford University Press, New York, 1989).

[12] H. Chen and A. Zhou, Numerical Mathematics: Theory, Methods and Applications **1**, 1 (2008), ISSN 2079-7338, URL <https://global-sci.com/article/90767/orbital-free-density-functional-theory-for-molecular-structure>.

[13] B. G. Radhakrishnan and V. Gavini, *Electronic Structure Calculations at Macroscopic Scales using Orbital-Free DFT* (????), pp. 147–163.

[14] W. Mi, A. Genova, and M. Pavanello, The Journal of Chemical Physics **148**, 184107 (2018), ISSN 0021-9606, URL <https://doi.org/10.1063/1.4972007>.

//doi.org/10.1063/1.5023926.

[15] L. A. Constantin, E. Fabiano, S. Śmiga, and F. Della Sala, Physical Review B **95** (2017), ISSN 2469-9969, URL <http://dx.doi.org/10.1103/PhysRevB.95.115153>.

[16] E. Smargiassi and P. A. Madden, Phys. Rev. B **49**, 5220 (1994), URL <https://link.aps.org/doi/10.1103/PhysRevB.49.5220>.

[17] Q. Xu, Y. Wang, and Y. Ma, Phys. Rev. B **100**, 205132 (2019), URL <https://link.aps.org/doi/10.1103/PhysRevB.100.205132>.

[18] L.-W. Wang and M. P. Teter, Phys. Rev. B **45**, 13196 (1992), URL <https://link.aps.org/doi/10.1103/PhysRevB.45.13196>.

[19] C. Herring, Phys. Rev. A **34**, 2614 (1986), URL <https://link.aps.org/doi/10.1103/PhysRevA.34.2614>.

[20] L. A. Constantin, E. Fabiano, and F. Della Sala, Physical Review B **97** (2018), ISSN 2469-9969, URL <http://dx.doi.org/10.1103/PhysRevB.97.205137>.

[21] W. Mi, K. Luo, S. Trickey, and M. Pavanello, Chemical Reviews **123** (2023).

[22] A. Bhattacharjee, S. Jana, and P. Samal, The Journal of Chemical Physics **160**, 224110 (2024), ISSN 0021-9606, https://pubs.aip.org/aip/jcp/article-pdf/doi/10.1063/5.0204957/19998017/224110_1_5.0204957.pdf, URL <https://doi.org/10.1063/5.0204957>.

[23] E. Prodan and W. Kohn, Proceedings of the National Academy of Sciences **102**, 11635 (2005), <https://www.pnas.org/doi/pdf/10.1073/pnas.0505436102>, URL <https://www.pnas.org/doi/abs/10.1073/pnas.0505436102>.

[24] Y. A. Wang, N. Govind, and E. A. Carter, Phys. Rev. B **60**, 17162 (1999).

[25] Y. A. Wang, N. Govind, and E. A. Carter, Phys. Rev. B **60**, 16350 (1999), URL <https://link.aps.org/doi/10.1103/PhysRevB.60.16350>.

[26] T. Kato, Communications on Pure and Applied Mathematics **10**, 151 (1957), <https://onlinelibrary.wiley.com/doi/pdf/10.1002/cpa.3160100201>, URL <https://onlinelibrary.wiley.com/doi/abs/10.1002/cpa.3160100201>.

[27] R. Ahlrichs, Journal of Mathematical Physics **14**, 1860 (1973), ISSN 0022-2488, https://pubs.aip.org/aip/jmp/article-pdf/14/12/1860/19224110/1860_1_online.pdf, URL <https://doi.org/10.1063/1.1666258>.

[28] E. Kryachko and E. Ludena (2015).

[29] R. O. Jones and O. Gunnarsson, Rev. Mod. Phys. **61**, 689 (1989), URL <https://link.aps.org/doi/10.1103/RevModPhys.61.689>.

[30] R. O. Jones, Rev. Mod. Phys. **87**, 897 (2015).

[31] H. Lee, C. Lee, and R. G. Parr, Phys. Rev. A **44**, 768 (1991), URL <https://link.aps.org/doi/10.1103/PhysRevA.44.768>.

[32] S. Laricchia, E. Fabiano, L. A. Constantin, and F. Della Sala, Journal of Chemical Theory and Computation **7**, 2439 (2011).

[33] L. A. Constantin, E. Fabiano, S. Laricchia, and F. Della Sala, Phys. Rev. Lett. **106**, 186406 (2011).

[34] T. Wang, K. Luo, and R. Lu, Journal of Chemical Theory and Computation **20**, 5176 (2024), pMID: 38861421, <https://doi.org/10.1021/acs.jctc.4c00532>, URL <https://doi.org/10.1021/acs.jctc.4c00532>.

[35] D. García-Aldea and J. E. Alvarellos, The Journal of Chemical Physics **127**, 144109 (2007), ISSN 0021-9606, https://pubs.aip.org/aip/jcp/article-pdf/doi/10.1063/1.2774974/15404367/144109_1_online.pdf, URL <https://doi.org/10.1063/1.2774974>.

[36] V. V. Karasiev, D. Chakraborty, O. A. Shukruto, and S. B. Trickey, Phys. Rev. B **88**, 161108 (2013), URL <https://link.aps.org/doi/10.1103/PhysRevB.88.161108>.

[37] K. Luo, V. V. Karasiev, and S. B. Trickey, Phys. Rev. B **98**, 041111 (2018), URL <https://link.aps.org/doi/10.1103/PhysRevB.98.041111>.

[38] K. Luo, V. V. Karasiev, and S. B. Trickey, Phys. Rev. B **101**, 075116 (2020), URL <https://link.aps.org/doi/10.1103/PhysRevB.101.075116>.

[39] L. A. Constantin, E. Fabiano, and F. Della Sala, The Journal of Physical Chemistry Letters **9**, 4385 (2018), pMID: 30019904, <https://doi.org/10.1021/acs.jpclett.8b01926>, URL <https://doi.org/10.1021/acs.jpclett.8b01926>.

[40] L. A. Constantin, E. Fabiano, and F. Della Sala, Journal of Chemical Theory and Computation **15**, 3044 (2019), pMID: 30964665, <https://doi.org/10.1021/acs.jctc.9b00183>, URL <https://doi.org/10.1021/acs.jctc.9b00183>.

[41] L. A. Constantin, Phys. Rev. B **99**, 155137 (2019), URL <https://link.aps.org/doi/10.1103/PhysRevB.99.155137>.

[42] C. Huang and E. A. Carter, Phys. Rev. B **81**, 045206 (2010), URL <https://link.aps.org/doi/10.1103/PhysRevB.81.045206>.

[43] W. Mi and M. Pavanello, Phys. Rev. B **100**, 041105 (2019), URL <https://link.aps.org/doi/10.1103/PhysRevB.100.041105>.

[44] X. Shao, W. Mi, and M. Pavanello, Phys. Rev. B **104**, 045118 (2021), URL <https://link.aps.org/doi/10.1103/PhysRevB.104.045118>.

[45] L. A. Constantin, A. Terentjevs, F. Della Sala, P. Cortona, and E. Fabiano, Phys. Rev. B **93**, 045126 (2016), URL <https://link.aps.org/doi/10.1103/PhysRevB.93.045126>.

[46] J. P. Perdew, Physics Letters A **165**, 79 (1992), ISSN 0375-9601, URL <https://www.sciencedirect.com/science/article/pii/037596019291058Y>.

[47] M. Levy and H. Ou-Yang, Phys. Rev. A **38**, 625 (1988), URL <https://link.aps.org/doi/10.1103/PhysRevA.38.625>.

[48] M. Hemanadhan and M. K. Harbola, The European Physical Journal D **66** (2012), ISSN 1434-6079, URL <http://dx.doi.org/10.1140/epjd/e2012-20677-4>.

[49] K. Finzel, The Journal of Chemical Physics **144**, 034108 (2016), ISSN 0021-9606, https://pubs.aip.org/aip/jcp/article-pdf/doi/10.1063/1.4940035/15507324/034108_1_online.pdf, URL <https://doi.org/10.1063/1.4940035>.

[50] A. Nagy, Phys. Rev. A **84**, 032506 (2011), URL <https://link.aps.org/doi/10.1103/PhysRevA.84.032506>.

[51] A. Nagy, The Journal of Chemical Physics **123**, 044105 (2005).

[52] J. J. Redd and A. C. Cancio, The Journal of Chemical Physics **155**, 134112 (2021), ISSN 0021-9606, https://pubs.aip.org/aip/jcp/article-pdf/doi/10.1063/5.0059283/16044182/134112_1_online.pdf, URL <https://doi.org/10.1063/5.0059283>.

[53] E. H. Lieb and B. Simon, Phys. Rev. Lett. **31**, 681 (1973), URL <https://link.aps.org/doi/10.1103/PhysRevLett.31.681>.

[54] J. J. Redd and A. C. Cancio, The Journal of Chemical Physics **155**, 134112 (2021), ISSN 0021-9606, https://pubs.aip.org/aip/jcp/article-pdf/doi/10.1063/5.0059283/16044182/134112_1_online.pdf, URL <https://doi.org/10.1063/5.0059283>.

[55] X. Shao, K. Jiang, W. Mi, A. Genova, and M. Pavanello, WIREs Computational Molecular Science **11** (2020), ISSN 1759-0884,

URL <http://dx.doi.org/10.1002/wcms.1482>.

[56] C. Huang and E. A. Carter, Phys. Chem. Chem. Phys. **10**, 7109 (2008), URL <http://dx.doi.org/10.1039/B810407G>.

[57] J. P. Perdew and Y. Wang, Phys. Rev. B **45**, 13244 (1992), URL <https://link.aps.org/doi/10.1103/PhysRevB.45.13244>.

[58] F. D. Murnaghan, Proceedings of the National Academy of Sciences **30**, 244 (1944), <https://www.pnas.org/doi/pdf/10.1073/pnas.30.9.244>, URL <https://www.pnas.org/doi/abs/10.1073/pnas.30.9.244>.

[59] A. Bhattacharjee, M. Harbola, H. Myneni, and P. Samal, supporting information (2025).

[60] Y. Wang, J. Lv, L. Zhu, and Y. Ma, Computer Physics Communications **183**, 2063 (2012), ISSN 0010-4655, URL <https://www.sciencedirect.com/science/article/pii/S0010465512001762>.

[61] Y. Wang, J. Lv, L. Zhu, and Y. Ma, Phys. Rev. B **82**, 094116 (2010), URL <https://link.aps.org/doi/10.1103/PhysRevB.82.094116>.

[62] J. Lv, Y. Wang, L. Zhu, and Y. Ma, The Journal of Chemical Physics **137**, 084104 (2012), ISSN 0021-9606, https://pubs.aip.org/aip/jcp/article-pdf/doi/10.1063/1.4746757/13989616/084104_1.online.pdf,

URL <https://doi.org/10.1063/1.4746757>.

[63] G. Kresse and J. Hafner, Phys. Rev. B **47**, 558 (1993).

[64] P. Giannozzi, S. Baroni, N. Bonini, M. Calandra, R. Car, C. Cavazzoni, D. Ceresoli, G. L. Chiarotti, M. Cococcioni, I. Dabo, et al., Journal of Physics: Condensed Matter **21**, 395502 (2009), URL <https://dx.doi.org/10.1088/0953-8984/21/39/395502>.

[65] B. Thapa, X. Jing, J. E. Pask, P. Suryanarayana, and I. I. Mazin, The Journal of Chemical Physics **158**, 214112 (2023), ISSN 0021-9606, https://pubs.aip.org/aip/jcp/article-pdf/doi/10.1063/5.0146167/17914336/214112_1_5.0146167.pdf, URL <https://doi.org/10.1063/5.0146167>.

[66] C. Huang and E. A. Carter, Phys. Rev. B **85**, 045126 (2012), URL <https://link.aps.org/doi/10.1103/PhysRevB.85.045126>.

[67] J. Xia and E. A. Carter, Phys. Rev. B **86**, 235109 (2012), URL <https://link.aps.org/doi/10.1103/PhysRevB.86.235109>.

[68] V. Rios-Vargas, X. Shao, S. B. Trickey, and M. Pavanello, Phys. Rev. B **110**, 085129 (2024), URL <https://link.aps.org/doi/10.1103/PhysRevB.110.085129>.

[69] G. S. Ho, V. L. Lignères, and E. A. Carter, Computer Physics Communications **179**, 839 (2008), ISSN 0010-4655, URL <https://www.sciencedirect.com/science/article/pii/S0010465508002476>.